SELF-AFFINE SNAKE: A NEW PARAMETRIC ACTIVE CONTOUR

M. Saadatmand-Tarzjan
saadatmand@ modares.ac.ir

H. Ghassemian
ghassemi@modares.ac.ir

Department of Electrical and Computer Engineering, Tarbiat Modares University,
P.O. Box 14115-194 Tehran, Iran

ABSTRACT

In this paper, a new active contour model called self-affine snake is proposed which integrates the self-affine mapping system (SAMS), wavelet transform, and snake model. It inherits wide capture range from the wavelet transform, both accurate fit to weak edges and effective reconstruction of boundary concavities from SAMS, and topological consistency from the snake model while avoiding their weak points. In self-affine snake, first, a force vector is computed for every pixel in each wavelet LL matrix using SAMS with disk domains. Then the obtained force fields of different wavelet scales are effectively combined to make the self-affine force filed. Finally, the snake is deformed using the resultant forces based on the snake dynamic formulation. Experiment results demonstrate good performance for self-affine snake compared to the balloon for a number of synthetic and biomedical benchmark images.

Index Terms— *Image shape analysis, wavelet transforms*

1. INTRODUCTION

The parametric active contours or snakes are parametric curves that can move toward desired features, usually edges, within an image domain under the influence of internal forces coming from within the curve itself and external forces derived from the image data [1]. The external forces usually draw the curve toward desired features while the internal forces hold the curve together (elasticity forces) and keep it from bending too much (bending forces). The external forces are divided into two categories: potential forces defined as the negative gradient of a potential function and dynamic forces formulated directly using a force balance formulation [2].

Snake models suffer three key difficulties: *i)* they should be usually initialized by an initial contour close to the object boundary [3], *ii)* they have difficulties to reconstruct the edge openings and progress into boundary concavities [4], and *iii)* they may likely converge to wrong results for weak edges, especially, when they lie beside strong edges [5]. However, most of methods introduced to address the above problems solve one problem while creating new difficulties. For example, multiresolution approaches increase the capture range of the external forces while deciding about how the contour should move across different resolutions is a challenging difficulty in such algorithms [4]. The balloon model addresses both the capturing range and boundary concavity problems using pressure forces, but they can not be too strong or weak edges will be overwhelmed [5]. Furthermore, the pressure forces are not bidirectional, a condition that mandates careful initialization. Another example is gradient vector flow and its variations [6-9] which effectively tackle the capturing range and boundary concavity problems though they may poorly perform for weak edges [10]. Additionally, they are computationally intensive due to computation of forces for almost all image pixels [11].

Considering the above difficulties, some researchers proposed several contour extraction algorithms that inherently differ from snakes. Ida and Yoko have been introduced a highly accurate method to approach and fit a roughly drawn line to the object contour using self-affine mapping systems [12]. The contractive self-affine mapping system has been typically used to produce fractal figures [13]. In an earlier work [14], Ida *et al* showed that edges attract mapping points during iterations of the map when they are initially set near them. They have utilized this attraction phenomenon to extract self-similar curves instead of a smooth curve like that in snakes. Ida's approach, in spite of significant strengths including accurate fit to boundaries and wide capture range, has some weak points. It sometimes abnormally deforms the contour due to fractal behaviors [12]. The authors addressed this drawback by defining the contour as a topologically-consistent parametric curve in an earlier work [15].

This work is an attempt to tackle the difficulties of both snake and Ida's algorithm by keeping their strengths while avoiding their weak points. In this paper, we propose a new parametric active contour model called self-affine snake which integrates the self affine mapping system (SAMS), wavelet transform, and snake model. Self-affine snake inherits wide capture range from the wavelet transform, both accurate fit to weak edges and effective reconstruction of boundary concavities from SAMS, and topological consistency from snakes.

This paper is organized as follows: in sections 2 and 3, the self-affine mapping system and snake model are reviewed, respectively. Section 4 presents the proposed self-affine snake. Experiment results are given in section 5. Finally, section 6 is devoted to concluding remarks.

2. SELF-AFFINE MAPPING SYSTEM

2.1 Contractive self-affine maps

Consider an image having the support $G\subset\boldsymbol{R}^2$ with intensity $g(\boldsymbol{x})$ for all $\boldsymbol{x}\in G$. The contractive map m_i with domain $M_i\subset G$ (i=1,…,I) is defined as follows:

$$m_i(\boldsymbol{x}) = r_i(\boldsymbol{x}-\tilde{\boldsymbol{x}}_i)+(\boldsymbol{\tau}_i+\tilde{\boldsymbol{x}}_i), \qquad r_i<1 \tag{1}$$

where $\tilde{\boldsymbol{x}}_i$ is the center point of M_i. The above equation translates M_i by vector $\boldsymbol{\tau}_i$=[s_i,t_i] and expands it by r_i to form domain W_i=m_i(M_i). A contractive self-affine model is defined as {M_i,m_i,u_i} where:

$$u_i(z) = p_i z + q_i, \quad z = m_i(\boldsymbol{x}), \quad 0\le p_i\le 1 \tag{2}$$

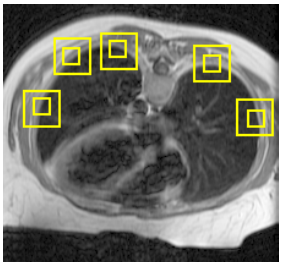

Figure 1. A self-affine model with *I=5* square domains.

2.2 Extracting self-affine maps

Extracting self-affine models includes two steps. First, some M_i are allocated. The allocation method depends on the application of self-affine model. Then, a search is performed to indicate the parameters of maps including r_i, s_i, t_i, p_i, and q_i using a block matching algorithm [13]. For each self-affine map, the block matching algorithm changes the value of one parameter in each step and then, a matching cost is evaluated as follows:

$$C = \sum\nolimits_{\boldsymbol{x}\in M_i} \left| g(\boldsymbol{x}) - g(m_i(\boldsymbol{x}))\right| \tag{3}$$

After checking all situations, the best set of values with the minimum cost is selected. Figure 1 illustrates a self-affine model with square domains, setting *I=5* and r_i=1/2. As shown, the texture in each larger block (M_i) is almost similar to that in the corresponding smaller block (W_i).

2.3 Extracting self-affine contours

To extract self-affine contours by Ida's algorithm, the square domains W_i are firstly initialized along an initial contour such that each domain almost covers half of each adjacent domain (see left image in Figure 2). Then, the self-affine maps attached to these domains are extracted using the block matching algorithm explained in Section 2.2. Finally, each point on the contour is mapped in each step by the surrounding self-affine maps. The distances between the contour points and object boundary reduces to half in each mapping. Hence, the contour fits the object boundary after a few mappings [12].

To increase the capture range in Ida's algorithm, primary domains are selected enough large. Once the algorithm converges, all domains are initialized again with half size along the resultant contour. After extracting the self-affine maps attached to the new domains, the mapping process is repeated anew. Figure 2 shows the results of Ida's algorithm for a flower image.

3. PARAMETRIC SNAKES

A traditional snake is a curve x(s)=[x(s),y(s)], s∈[0,1] that moves in the spatial domain of an image to minimize the energy functional [1]:

$$E = \int_0^1 \frac{1}{2}\left[\alpha\left|\boldsymbol{x}'(s)\right|^2 + \beta\left|\boldsymbol{x}''(s)\right|^2\right] + E_{\text{ext}}(\boldsymbol{x}(s))ds \tag{4}$$

where $\boldsymbol{x}'(s)$ and $\boldsymbol{x}''(s)$ are the first and second derivatives of $\boldsymbol{x}(s)$ with respect to s and the weighting parameters α and β control the snake tension and rigidity, respectively. The external energy function E_{ext} derived from the image takes on smaller values at interested features such as object boundaries. A snake that minimizes E must satisfy the Euler equation given by:

$$\alpha\boldsymbol{x}''(s) - \beta\boldsymbol{x}^{(4)}(s) - \nabla E_{\text{ext}} = 0 \tag{5}$$

Defining $\mathbf{F}_{\text{int}}^{(\text{p})} = \alpha\boldsymbol{x}''(s) - \beta\boldsymbol{x}^{(4)}(s)$ and $\mathbf{F}_{\text{ext}}^{(\text{p})} = -\nabla E_{\text{ext}}$, we have the following force balance equation:

$$\mathbf{F}_{\text{int}} + \mathbf{F}_{\text{ext}}^{(\text{p})} = 0 \tag{6}$$

where the internal force $\mathbf{F}_{\text{int}}$ discourages stretching and bending while the external potential force $\mathbf{F}_{\text{ext}}^{(\text{p})}$ pushes the snake toward the desired image features. A solution to (6) is found by setting the left hand side of (6) equal to the derivative of the snake $\boldsymbol{x}$ with respect to time:

$$\boldsymbol{x}_t(s,t) = \alpha\boldsymbol{x}''(s) - \beta\boldsymbol{x}^{(4)}(s) - \nabla E_{\text{ext}} \tag{7}$$

When the solution $\boldsymbol{x}(s,t)$ stabilizes, the term $\boldsymbol{x}_t(s,t)$ vanishes and we achieve the solution of (6).

Several researchers directly formulate the snake using a force balance equation in which the standard external potential force $\mathbf{F}_{\text{ext}}^{(\text{p})}$ is replaced by a more general external force $\mathbf{F}_{\text{ext}}^{(\text{g})}$ as follows [2, 11]:

$$\mathbf{F}_{\text{int}} + \mathbf{F}_{\text{ext}}^{(\text{g})} = 0 \tag{8}$$

where $\mathbf{F}_{\text{ext}}^{(g)}$ is usually a combination of potential and (non-potential) dynamic forces.

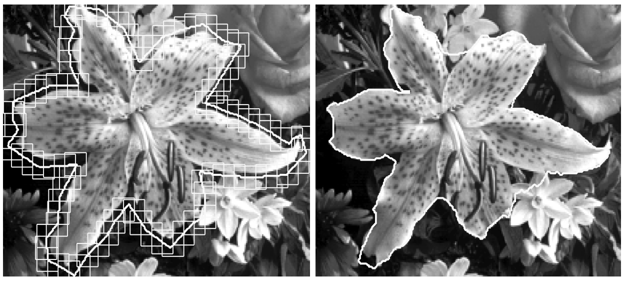

Figure 2. The initial contour and square domains (left) and the final contour obtained by Ida's algorithm (right).

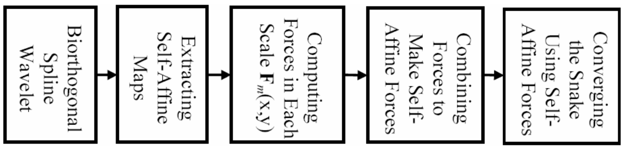

Biorthogonal Spline Wavelet

Extracting Self-Affine Maps

Computing Forces in Each Scale $\mathbf{F}_m(x,y)$

Combining Forces to Make Self-Affine Forces

Converging the Snake Using Self-Affine Forces

Figure 3. Block diagram of the proposed self-affine snake.

4. PROPOSED APPROACH

The proposed self-affine snake algorithm integrates the snake model, SAMS, and wavelet transform to keep their strengths and avoid their weak points. As shown in Figure 3, the algorithm consists of five steps: *i)* computing wavelet transform, *ii)* extracting self-affine maps in each scale, *iii)* computing forces for each scale, *iv)* combining the forces of different scales to make self-affine forces, and *v)* converging the snake model using the obtained forces.

4.1 Computing wavelet transform

Ida's algorithm uses square domains with different sizes to increase the capture range. Instead, extracting the self-affine maps with small domain size in different scales of an image can obviously reduce the computational cost. Hence, we compute the discrete wavelet transform of the input image in *n* consecutive scales using compactly supported biorthogonal spline wavelets for which symmetry and exact reconstruction are possible with FIR filters [16].

4.2 Extracting self-affine maps

After computing the wavelet coefficients, a self-affine map is extracted for each pixel of LL submatrix in each scale. In other words, each pixel is attached to a self-affine map. As shown in Figure 4, we use circular domains for their symmetry in all directions. The domain $M_{x,y}$ corresponded to the pixel $\boldsymbol{x}$=(x,y) is a circle with radius of R pixels and centre at $\boldsymbol{x}$. The parameters of all self-affine maps are extracted by the block matching algorithm (see Section 2.2). In order to reduce the computational intensity of the block matching algorithm, the parameters $r_{x,y}$, $p_{x,y}$, and $q_{x,y}$ are set equal to 1/2, 1, and 0, respectively. Also, the range of variations of parameters $s_{x,y}$ and $t_{x,y}$ are defined as $[x\text{-}R/2,x+R/2]$ and $[y\text{-}R/2,y+R/2]$, respectively, for domain $M_{x,y}$.

4.3 Computing forces for each scale

The block matching algorithm computes the best translation vector $\boldsymbol{\tau}_{x,y}=[s_{x,y},t_{x,y}]$ which minimizes the matching cost between domains $M_{x,y}$ and $W_{x,y}$. Considering this fact that the object boundaries attract the self-affine maps [14], $\boldsymbol{\tau}_{x,y}$ may give the best direction to move the active contour at pixel $\boldsymbol{x}=(x,y)$. Hence, we define the forces of the m-th wavelet scale as follows:

$$\mathbf{F}_m^{(\mathrm{g})}(x,y)=\frac{\boldsymbol{\tau}_{x,y}^m}{\left|\boldsymbol{\tau}_{x,y}^m\right|}\left(\frac{|LH_m(x,y)|+|HL_m(x,y)|}{\max\limits_{(x,y)}(|LH_m(x,y)|+|HL_m(x,y)|)}\right) \tag{9}$$

where $\boldsymbol{\tau}_{x,y}^m$ is the translation vector given by the block matching algorithm for pixel (x,y) in LL submatrix of the m-th wavelet scale. Furthermore, LH_m and HL_m indicate LH and HL submatrices of the m-th wavelet scale. According to (9), forces are scaled by the normalized gradient amplitude.

4.4 Combining forces

To compute the proposed self-affine forces, the forces of different wavelet scales should be effectively combined. We use a weighted superposition for this aim. The self-affine force is computed for pixel $\boldsymbol{x}=(x,y)$ in the image domain as follows:

$$\mathbf{F}_{\mathrm{SAM}}^{(\mathrm{g})}(x,y)=\hat{\mathbf{F}}_{\mathrm{GSN}}^{(\mathrm{p})}(x,y)+\sum\nolimits_{m=1}^{n}2^{-m}\times\mathbf{F}_m^{(\mathrm{g})}(\frac{x}{2^m},\frac{y}{2^m}) \tag{10}$$

where $\hat{\mathbf{F}}_{\mathrm{GSN}}^{(\mathrm{p})}$ is given by:

$$\hat{\mathbf{F}}_{\mathrm{GSN}}^{(\mathrm{p})}(x,y)=\begin{cases}\dfrac{\mathbf{F}_{\mathrm{GSN}}^{(\mathrm{p})}(x,y)}{\max\limits_{(x,y)}\left(\left|\mathbf{F}_{\mathrm{GSN}}^{(\mathrm{p})}(x,y)\right|\right)} & \dfrac{\left|\mathbf{F}_{\mathrm{GSN}}^{(\mathrm{p})}(x,y)\right|}{\max\limits_{(x,y)}\left(\left|\mathbf{F}_{\mathrm{GSN}}^{(\mathrm{p})}(x,y)\right|\right)}>\theta \\ 0 & \text{Ortherwise}\end{cases} \tag{11}$$

where $\mathbf{F}_{\mathrm{GSN}}^{(\mathrm{p})}(x,y)=-\nabla\left(-\left|\nabla\left[G_\sigma(x,y)*g(x,y)\right]\right|^2\right)$ indicates Gaussian potential forces [2] that are used in order to improve the boundary localization performance of self-affine forces.

4.5 Converging snake model

The resultant self-affine forces are then used to move the active contour toward the object boundary according to the dynamic snake formulation (see Eq. 8).

In all demonstrated experiments in this paper, self-affine forces are computed for all image pixels to make a complete force field. However, they can be equivalently computed only for pixels on the current curve in each step. It means that the computational intensity of self-affine snake can be significantly decreased by this manner.

4.6 Number of wavelet scales

According to (10), the capture range of self-affine forces is increased by increasing the number of wavelet scales, n. Generally, in order to capture the snake from distance L, the number of wavelet scales is simply given by:

$$2^n\times R>L\Rightarrow n>\log_2(L/R) \tag{12}$$

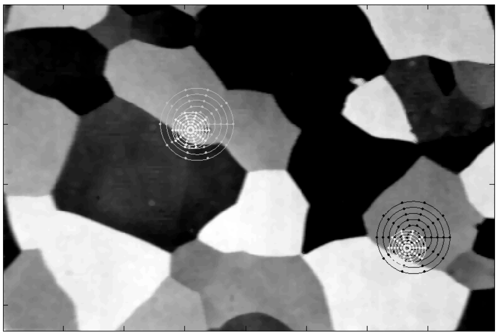

Figure 4. Two illustrations of circular domains used in self-affine snake. Textures in the larger and smaller circles are similar for each pair.

5. RESULTS AND DISCUSSION

We performed a large number of experiments to study the performance of the proposed self-affine snake algorithm. In all experiments, R and θ were set to 5 and 0.2, respectively. We first note that for all experiments, the traditional potential forces such as Gaussian forces were too weak to overpower the internal forces and the snake shrank at the centre of the figure. Furthermore, self-affine snake in contrast to Ida's algorithm was usually topologically-consistent in all experiments due to the parametric definition of curve (results not shown).

Figure 5 illustrates the self-affine forces for a synthetic image with openings at top and bottom. The convergence of self-affine snake for this image compared to a balloon model with an outward pressure force is shown in Figure 6. The self-affine forces are bidirectional and they provide an adequate wide capture range. Furthermore, self-affine snake could effectively progress into boundary concavities and it reconstructed the subjective boundaries at the top and bottom as well. Clearly, the pressure forces caused the balloon model to bulge outward through the openings at top and bottom and hence, the subjective contours were not reconstructed well. Figure 7 and 8 demonstrate similar results for a cell image with weak boundaries close to the strong edges of the cell centre. Figure 9 shows the convergence of self-affine snake with three different initializations for a magnetic resonance (MR) image of left ventricle of a human heart. As shown, self-affine snake effectively converged to subjective contours for all of them.

6. CONCLUDING REMARKS

In this paper, a new active contour model called self-affine snake was proposed. It integrates the wavelet transform, self-affine mapping system, and snake model to keep their strengths while avoiding their drawbacks. Although self-affine snake demonstrated good performance for parametric active contours in this paper, we expect that it has applications in geometric active contours as well. How this can be achieved is an open problem and further research is necessary to this end.

7. REFERENCES

[1] M. Kass, A. Witkin, D. Terzopoulos, "Snakes: active contour models", *Intern. J. Comp. Vision,* 1(4):321-331, 1987.

[2] C. Xu, D. Pham, J. L. Prince, "Image segmentation using deformable models", In J. Fitzpatrick and M. Sonka (editors), *Handbook of Medical Imaging*. vol. 2: *Medical Image Processing and Analysis*, pp. 175-272, London, 2000.

[3] C. Xu, J.L. Prince, "Generalized gradient vector flow external forces for active contours," *Signal Processing*, 71:131-139, 1998.

[4] B. Leroy, I. Herlin, L. D. Cohen, “Multi-resolution algorithms for active contour models”, *12th Int’l Conf. Analysis and Optimization of Systems*, pp. 58-65, 1996.

[5] L. D. Cohen, “On active contour models and balloons”, *CVGIP: Image Understanding*, 53:211-218, 1991.

[6] C. Xu, J.L. Prince, “Generalized gradient vector flow external forces for active contours,” *Signal Processing*, 71:131-139, 1998.

[7] C. Lia, J. Liub, and M.D. Foxa, “Segmentation of external force field for automatic initialization and splitting of snakes,” *Pattern Recognition*, 38:1947-1960, 2005.

[8] C. Lia, J. Liub, and M.D. Foxa, “Segmentation of external force field for automatic initialization and splitting of snakes,” *Pattern Recognition*, 38:1947-1960, 2005.

[9] N. Jifeng, W. Chengke, L. Shigang, Y. Shuqin, “NGVF: An improved external force field for active contour model,” *Pattern Recognition Letters*, 28:58-63, 2007.

[10] X. Xie, M. Mirmehdi, “RAGS: Region-aided geometric snake”, *IEEE Trans. Image Processing*, 13(5):640-652, 2004.

[11] C. Xu, J. L. Prince, “Snakes, shapes, and gradient vector flow”, *IEEE Trans. Image Processing*, 7(3):359-369, 1998.

[12] T. Ida, Y. Sambonsugi, “Self-affine mapping system and its application to object contour extraction”, *IEEE Trans. Image Processing*, 9(11):1926-1936, 2000.

[13] M. Barnsley, L. Hurt, *Fractal Image Compression*. Wellesley, MA: Peters, 1993.

[14]T. Ida, Y. Sambonsugi, “Image segmentation and contour detection using fractal coding”, *IEEE Trans. Circuits Syst. Video Technol.*, 8:968-975, 1998.

[15] M. Saadatmand-Tarzjan, H. Abrishami Moghaddam, “A new method for contour extraction based on self-affine mapping system”, *Conf. Intelligent Systems (CIS’04)*, 2004. (in Farsi)

[16] I. Daubechies, “Ten lectures on wavelets”, CBMS, SIAM, 61:271-280, 1994.

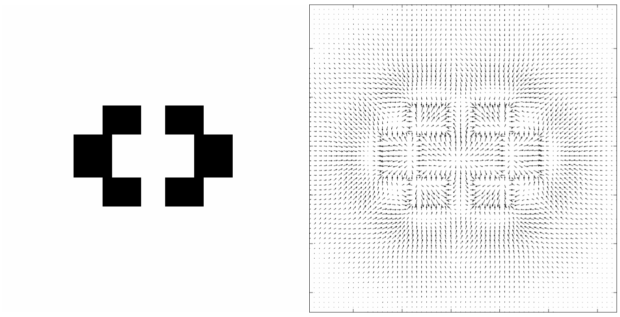

Figure 5. The proposed self-affine forces (right) for a synthetic 64×64-pixel image (left) with openings at top and bottom.

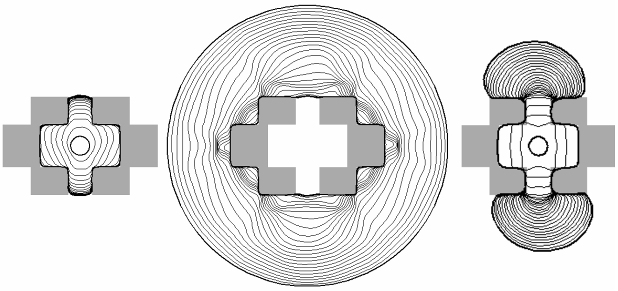

Figure 6. Convergence of self-affine snake with two different initializations (left and middle) for the image shown in Figure 5-left compared to a balloon model with an outward pressure force (right).

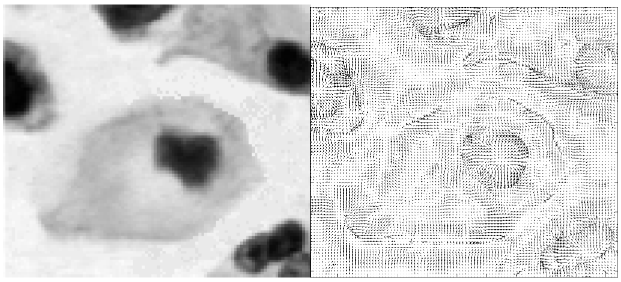

Figure 7. The proposed self-affine forces (right) for a 104×92-pixel cell image (left) with weak boundaries close to strong edges.

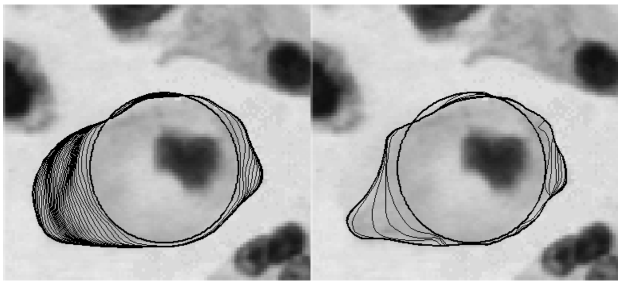

Figure 8. Convergence of Self-affine snake (right) for the image shown in Figure 7-left compared to a balloon model with an outward pressure force (left).

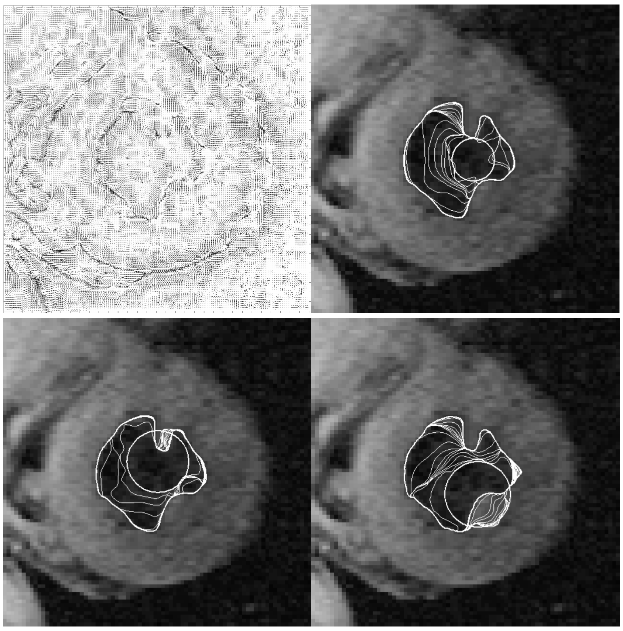

Figure 9. The proposed self-affine forces (top-left) for a 160×160-pixel MR image of left ventricle of a human heart and convergence of Self-affine snake with three different initializations.